Journal of Polymer Research (2020) 27:71
https://doi.org/10.1007/s10965-020-2037-5

ORIGINAL PAPER

Synthesis and characterization of GO doped bio-resource based composites for NLO and multifaceted applications

V. Selvaraj[1] · K. P. Jayanthi[1] · K. Arunkumar[1] · S. Jeyaram[2] · T. Geethakrishnan[2] · M. Alagar[3]

Received: 28 September 2019 / Accepted: 7 February 2020

Abstract

The objective of the present work is to synthesize three different types of cardanol based benzoxazines such as cardanol-{1,4-bis(4-aminophenoxy)ethane}benzoxazine ($CBAE_2Bz$), cardanol-{1,4-bis(4-aminophenoxy)butane} benzoxazine ($CBAE_4Bz$) and cardanol-{1,4-bis(4-aminophenoxy)octane}benzoxazine ($CBAE_8Bz$) by varying aliphatic ether link chain length through solventless method. The benzoxazines obtained with varying chain length were converted in to three different types of composites using paraphenylenediamine (PPDA) functionalized gaphene oxide (*f*-GO) as nano-reinforcement with varying weight percentage and were characterized by different analytical techniques. The molecular structure of the monomers was confirmed from Fourier transform infrared (FTIR) spectroscopy, ^{1}HNMR, ^{13}C NMR and MALDI mass. Data obtained from thermal studies infer that the prepared composites possess good thermal stability and enhanced values of Tg with respect to weight percent of functionalized graphene oxide content. However, the values of thermal stability, Tg, dielectric constant and dielectric loss were marginally decreased with respect to increase in length of the spacer aliphatic chain. The SEM and TEM studies confirm the homogeneous dispersion and single layer thickness of graphene sheet, respectively. The feasibility of usage of *f*-GO/$PCAE_2Bz$ composite in both gram positive bacteria (*Bacillus subtilis, Staphylococcus aureus) and* gram negative bacteria (*Pseudomonas aeruginosa, Escherichia coli*) environments were checked and the results obtained were discussed. Further, third-order NLO properties of open and closed aperture Z–scan results conclude that GO doped bio-resource based composites exhibit saturable absorption and self-defocusing type optical non-linearity. The third-order NLO susceptibility (χ^3) of GO doped bio-resource based composites are increased with respect to quantity of reinforcement of GO to bio-based polymer. The maximum value of $1.03X\ 10^{-4}$ esu was observed and this nonlinearity is thermal in nature. Thus, the prepared composites may find wide range of applications in diverse surrounding conditions.

Keywords Cardanol based benzoxazine · Amine-functionalized graphene oxide · Thermal stability · Dielectric properties · Antifouling · NLO

Introduction

Dielectrics are insulating materials used in capacitor, power transformers, cables and transducers, etc. Generally polymers are considered to be dielectric materials and dielectric polarization usually occurs in the presence of electric field. The weak attractions exist between the nucleus and valence electrons contribute to polarization and also reoriented according to the charge of the electric field [1]. Normally, the incorporation of fillers in the polymers may cause interfacial polarization [2] and due to such interfacial polarization, a high dielectric constant is obtained even at low filler content [3]. Polybenzoxazine resin is one of the most important thermosetting phenolic polymer resins with unique properties such as low water absorption, high glass transition temperature, thermal stability.cures without any catalyst, zero volume

Electronic supplementary material The online version of this article (https://doi.org/10.1007/s10965-020-2037-5) contains supplementary material, which is available to authorized users.

✉ V. Selvaraj
vaithilingamselvaraj@gmail.com; vselva@aucev.edu.in; rajselva_77@yahoo.co.in

[1] Nanotech Research Laboratory, Department of Chemistry, University College of Engineering Villupuram (A Constituent College of Anna University, Chennai), Kakuppam, Villupuram, Tamilnadu 605 103, India

[2] Department of Physics, University College of Engineering Villupuram, Villupuram, Tamilnadu 605 103, India

[3] Polymer Engineering Laboratory, PSG Institute of Technology and Applied Research, Neelambur, Coimbatore 641062, India

Published online: 22 February 2020

shrinkage, high resistance to moisture, chemicals and UV light [4, 5], which find variety of applications ranging from electronics to aerospace. The benzoxazine compounds synthesized from phenolic resin, aromatic amines and formaldehydes have lower values of dielectric constant.

Cardanol acquired from bio-resources like cashew nut shells is a novel type of phenolic compound, in which the researchers were interested to obtained value added products and this is because it is generally treated as a waste in the cashew nut industry. Polybenzoxazines synthesized from cardanol is expected to overcome many of the deficiencies that are commonly associated with traditional phenolic resins [6–9]. The high thermal stability, high Tg, good mechanical and dielectric properties, low water absorption and good solubility in common organic solvents make the cardanol based benzoxazine suitable for high performance composites [10–12]. The high performance hybrid composites obtained by using organic matrix phase and inorganic fillers has attracted increasing interest due to their potential applications in the automotive, construction, aerospace and electronic industries [13–15].

Thus, the fillers like layer double hydroxides (LDH) [16], silica materials [17], montmorillonite based nanoclays [18] and carbon based nanofillers such as carbon black, carbon nanotubes (CNT) and carbon nano fibers (CNF) are playing significant role in the preparation of polymer composites [19–22]. Though CNT material has proven to be very effective as conductive fillers, the production cost is very high [23]. Hence, the researchers are changed their focus on graphite based reinforcement/fillers for the fabrication of polymer composites.

Graphite is a three dimensional carbon based material, which on oxidation generates oxygen based functionalities like -OH, -COOH, epoxy, -C=O, etc., in its structure. Graphene oxide is a two-dimensional sheet composed of sp2 carbon atoms with one atomic thickness. The presence of oxygen functionalities like epoxide, -OH, -COOH, -C=O, etc., makes it as an effective reinforcement/filler for ceramic and polymer matrices. The properties like good mechanical, electrical, high aspect ratio and low density of graphene oxide are comparable to those of carbon nanotube, which made it an ideal component to develop graphene oxide reinforced composites [24, 25]. The carbon based materials is also moderately toxic to most living cells, which were used as reinforcing material in polymer matrix to show its potential application in antimicrobial studies [26, 27]. The antimicrobial activity of graphene oxide may be attributed due to the generation of reactive oxygen species (ROS), which may cause cellular toxicity.

Usually, organic and inorganic compounds are distinguishable optical materials, which exhibits better third-order optical nonlinearities and quick response time [28–31]. Recently, polymer based NLO compounds have attracted much attention due to their distinguishable optical qualities and significant third-order nonlinearities [32–35]. Such polymer based composite materials have potential applications in biosensors, optoelectronic devices, light emitting diodes, coatings and storage devices [36, 37].

With these view in mind, graphene oxide functionalized with paraphenylene diamine was used as a reinforcement for the new type of cardanol based aliphatic ether linked benzoxazine polymer composites. The cardanol based aliphatic ether linked benzoxazine monomer was obtained using cardanol, aromatic diamines with different alkoxy chain lengths (CAE_nBz, $n = 2$, 4 and 8). The comparative studies were carried out for thermal and dielectric properties to ascertain the influence of aliphatic ether chain length. Further, antimicrobial activities of $PCBAE_2Bz$ matrix and *f*-GO/$PCBAE_2Bz$ composites against *E.coli, P.aeruginosa, S. aureus* and *Bacillus subtilis* were carried out with well diffusion method. In addition, the third-order NLO properties and their optical limiting characteristics are done using Z–scan method. To the best of our knowledge, no article of this type has published yet. In this work, an attempt has been made to study the NLO behavior of an agro-waste based benzoxazine polymer. The experimental results of Z–scan measurements for third-order NLO properties and optical limiting behavior in non-aqueous solutions under 5 mW diode laser at 635 nm are discussed and reported.

Experimental methods

Materials

Graphite was purchased from Active Carbon India Pvt.Ltd., India. Hydrogen peroxide (H_2O_2) was purchased from SD Fine Chemicals, India. Potassium permanganate ($KMnO_4$) and sodium nitrate ($NaNO_3$) were purchased from Merck. Paraformaldehyde, THF, ethanol, diethyl ether (99.5%), H_2SO_4 (95%) and HNO_3 (70%) were procured from SRL India. Para phenylene diamine, 1-chloro-4-nitro benzene, 1,2-ethanediol, 1,4-butanediol and 1,8-octanediol were obtained from Sigma Aldrich. Cardanol was purchased from Sathya cashew chemicals Pvt. Ltd., Chennai.

Synthesis of linear aliphatic ether linked aromatic dinitro compounds (AE_nADN)

1,2-bis(4-nitrophenoxy)ethane (C_2NO_2), 1,4-bis(4-nitrophenoxy)butane (C_4NO_2) and 1,8-bis(4-nitrophenoxy)octane (C_8NO_2) were synthesized by reacting 1, 2- ethanediol, 1,4-butanediol and 1,8 octanediol separately with 1-chloro-4-nitrobenzene in the presence of NaH as catalyst. Typically, 100 mL of dry dimethylformamide (DMF),

30 g of sodium hydride and 10 g (0.1611 mol) of 1, 2 ethanediol were taken in a 250 mL round bottomed flask. The whole mixture was stirred for 3 h at 50 °C and cooled in an ice bath (0-5 °C) to get the sodium salt of diol. To the above reaction mixture, 50.7 g (0.3222 mol) of 1-chloro-4-nitrobenzene dissolved in 100 mL DMF was slowly added at the same temperature and then the temperature was raised to 30 °C and then stirring was continued for overnight. Finally, the reaction product was quenched with crushed ice, filtered and washed with distilled water followed by chilled isopropanol (Scheme 1). 1,4-bis(4-nitrophenoxy)butane (C_4NO_2) and 1,8-bis(4-nitrophenoxy)octane (C_8NO_2) were also synthesized using the same procedure by using 1,4-butanediol and 1,8- octane diol respectively with1-chloro-4-nitrobenzene instead of 1, 2 - ethanediol.

Synthesis of linear aliphatic ether linked aromatic diamine compounds (AE_nADA)

1,2-bis (4-aminophenoxy)ethane (C_2NH_2), 1,4-bis(4-aminophenoxy)butane (C_4NH_2) and 1,8-bis(4-aminophenoxy)octane (C_8NH_2) were prepared by reducing the 1,2-bis(4-nitrophenoxy)ethane (C_2NO_2), 1,4-bis(4-nitrophenoxy)butane (C_4NO_2) and 1,8-bis(4-nitrophenoxy)octane (C_8NO_2) with Pd/C catalyst. Normally, 10 g of aliphatic ether linked nitro compound like 1,2-bis(4-nitrophenoxy)ethane (C_2NO_2) or 1,4-bis(4-nitrophenoxy)butane (C_4NO_2) or 1,8-bis(4-nitrophenoxy)octane (C_8NO_2), 100 mL of ethanol and 1 g of 10% Pd/C were taken in a 250 mL round bottomed flask. The temperature of the reaction mixture was raised to 50 °C and then 20 mL of hydrazine hydrate was added to the mixture. The resultant reaction mixture was refluxed for 3 h. The product obtained was filtered in hot condition and then cooled to room temperature to get white crystals. 1,4-bis(4-aminophenoxy)butane (C_4NH_2) and 1,8-bis (4-aminophenoxy)octane (C_8NH_2) were also synthesized by adopting similar reaction procedure by reducing 1,4-bis(4-nitrophenoxy)butane (C_4NO_2) and 1,8-bis(4-nitrophenoxy)octane (C_8NO_2) nitro compound, respectively.

Synthesis of aliphatic ether linked cardanol based benzoxazine monomer ($CBAE_nBz$)

Cardanol based aliphatic ether linked benzoxazine monomers ($CBAE_nBz$) with varying alkoxy chain ($n = 2, 4$ and 8) lengths were synthesized by using a single step condensation reaction of respective diamines (1,2-bis(4-aminophenoxy)ethane 1,4-bis(4-aminophenoxy)butane and 1,8-bis(4-aminophenoxy)octane), cardanol and paraformaldehyde by following a solventless method. For $CBAE_2Bz$ monomer preparation, mixture of cardanol (12.21 g, 0.04 mol), paraformaldehyde (2.58 g, 0.085 mol), and 1,2-bis(4-aminophenoxy)ethane (5 g, 0.020 mol) were taken in a round-bottomed flask equipped with a magnetic stirrer and refluxing condenser. The resulted reaction mixture was refluxed at 85 °C for 1 h and at 130 °C for 5 h. On cooling, chloroform (100 mL) was added and organic layer was washed with an aqueous sodium hydroxide (2 N) followed by distilled water. The organic layers were combined, dried over sodium sulphate and filtered. The solvent was removed under reduced pressure and the product obtained was dried at 353 K under vacuum to get $CBAE_2Bz$ as yellowish brown solid (Scheme 2).

Further, $CBAE_4Bz$ and $CBAE_8Bz$ monomers were synthesized using the same procedure by taking a mixture of cardanol (4.38 g, 0.012 mol), paraformaldehyde (0.926 g, 0.030 mol),and1,4bis(4-aminophenoxy) butane (2 g, 0.0073 mol) for $CBAE_4Bz$ and cardanol(1.84 g,0.012 mol),paraformaldehyde (0.926 g, 0.0012 mol), and 1,8-bis(4-aminophenoxy)octane(2 g,0.0061 mol)for$CBAE_8Bz$ monomers.

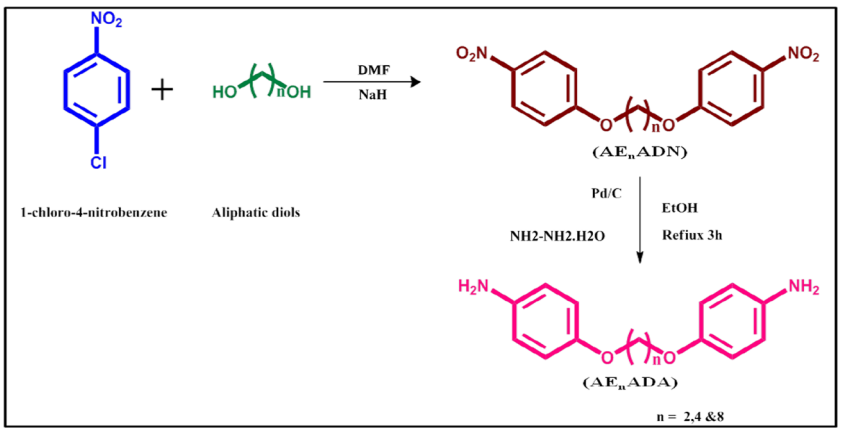

Scheme 1 Synthesis of aliphatic ether linked aromatic diamines (AE_nADA).

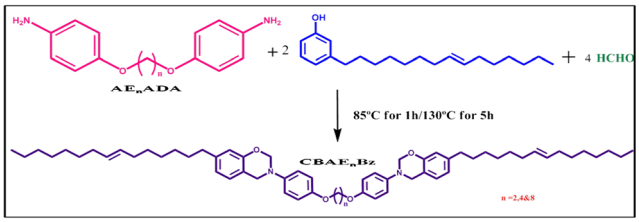

Scheme 2 Synthesis of aliphatic ether linked cardanol based benzoxazine.

Synthesis of graphene oxide (GO) and functionalized graphene oxide (*f*-GO)

Graphene oxide was synthesized by Hummer's method through the oxidation of graphite powder as reported earlier [38]. Graphite flakes (2 g) and $NaNO_3$ (2 g) were mixed in 50 mL of H_2SO_4 (98%) in a 1000 mL volumetric flask and kept under an ice bath (0–5 °C) with continuous stirring. The stirring was continued for another 2 h. The potassium permanganate (6 g) was slowly added and the addition was done carefully by keep the reaction temperature lower than 15 °C. The ice bath was then removed and the reaction mixture was stirred at 35 °C until it became brownish color and kept stirring for another 2 days. The reaction mixture was then diluted slowly with 100 mL of water in an ice bath. The reaction temperature was rapidly increased to 98 °C with effervescence and this solution was further diluted by adding additional 200 mL of water under continuous stirring. Finally, the solution is treated with 10 mL H_2O_2 and the solution becomes yellow in color. The resultant reaction mixture was centrifuged and washed with 10% HCl followed by de-ionized water. The obtained solid graphene oxide was dried under vacuum at room temperature.

Synthesis of paraphenylene diamine functionalized graphene oxide (*f*-GO)

To increase the compatibility of graphene oxide (GO) with polybenzoxazine, the graphene oxide is treated with an aromatic diamine viz., pare phenylene diamine (PPDA). Typically, 250 mg of GO is dispersed in 100 mL distilled water (100 mL) in a round bottomed flask and then sonicated for 2 h. 1.0126 g of pare phenylene diamine (PPDA) dissolved in 30 mL of warm distilled water (~70 °C) was added to the above dispersion and thus the ratio of GO and PPDA was maintained as 1:5. The resulted reaction mixture was again sonicated for another 2 h and then heated to 80 °C for 30 min under magnetic stirring condition. The excess amount of diamine was used to ensure the completion of reaction of amine groups with carboxyl groups on GO and to have amine groups on the surface of GO. The final product was centrifuged, and washed with water to remove the excess PPDA (Scheme 3).

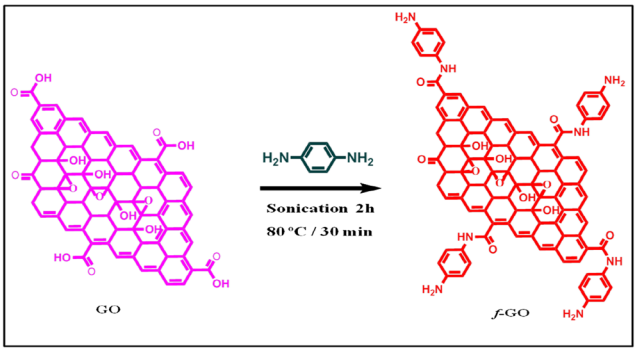

Scheme 3 Synthesis of paraphenylene diamine functionalized graphene oxide (*f*-GO)

Preparation of paraphenylene diamine functionalized graphene oxide (*f*-GO) incorporated aliphatic ether linked cardanol based polybenzoxazine ((*f*-GO/PCBAE$_n$Bz) composites

About 2 g of CBAE$_n$Bz monomer was dissolved in 5 mL $CHCl_3$.To this, the varying weight percentages of *f*-GO (1%, 3% and 5 wt.%) dispersed in $CHCl_3$ were added gradually to the benzoxazine monomer solution under sonication and the sonication was continued for further one hour. The obtained solutions were poured separately into a respective silane coated glass plates and cured at 120 °C for 1 h, 160 °C for 1 h, 180 °C for 1 h, 200 °C for 2 h, and 220 °C for 2 h to get a semi transparent *f*-GO/PCBAE$_n$Bz composite films (Scheme 4).

Further, aliphatic ether linked cardanol based polybenzoxazine (PCBAE$_n$Bz) polymers were prepared by taking their respective CBAE$_n$Bz monomers and cured at 120°Cfor 1 h, 160 °C for 1 h, 180 °C for 1 h, 200 °C for 2 h, and 220 °C for 2 h to get a transparent polymer film for comparative studies.

Antimicrobial studies

The antibacterial activities of all test compounds such as PCBAE$_2$Bz, 1%*f*-GO/PCBAE$_2$Bz, 3%*f*-GO/PCBAE$_2$Bz and 5%*f*-GO/PCBAE$_2$Bz were carried out by well diffusion method (Figs. 1, 2, 3, 4, 5, 6, 7, 8, 9, 10, 11, 12, 13, 14, 15, 16, 17). DMSO was used as the solvent and the test compounds were taken in the concentration range of 6.25, 12.5, 25, 50 μg/mL. The target microorganisms were cultured in Mueller–Hinton broth (MHB). After 24 h, the suspensions were adjusted to standard sub-culture dilutions. The petri dishes contains Muller Hinton Agar (MHA) medium. The agar plates were seeded with freshly prepared different pathogens. Agar wells with diameter of 6 mm were made with the help of a sterile stainless steel cork borer. The standard drug streptomycin (10 μg) was used as a positive reference standard to determine the sensitivity of each microbial species tested. Then the plates were incubated at 37 °C for 24 h. The diameter of the clear zone around the disc was measured and expressed in millimeters as theirs anti-microbial activity.

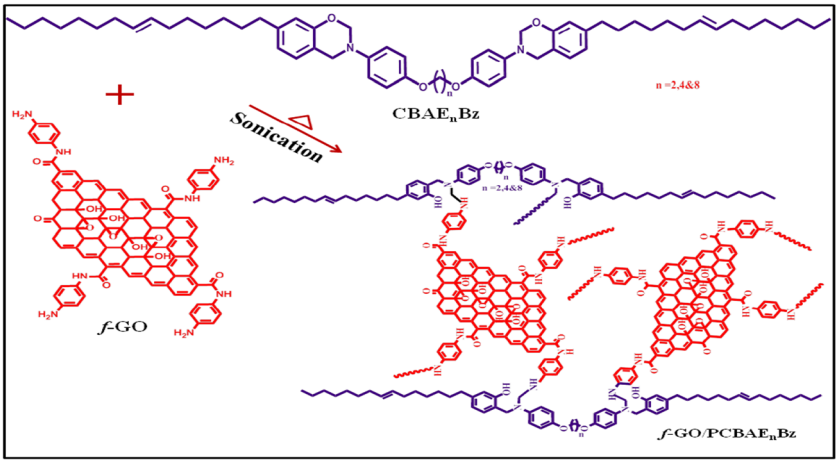

Scheme 4 Paraphenylene diamine functionalized graphene oxide (*f*-GO) incorporated aliphatic ether linked cardanol based polybenzoxazine (PCBAE$_n$Bz) composites synthesis of (*f*-GO/PCBAE$_n$Bz) composites.

Characterization techniques

FT-IR spectra were measured with the wave number ranges from 4000 to 500 cm^{-1} at the resolution of 0.1 cm^{-1} by making KBr disc for the prepared sample on Perkin Elmer 6X FT IR spectrometer. Raman spectra are recorded using 1064 nm line of Nd:YAG laser as the excitation wavelength range of 500–2500 cm^{-1} on a Thermo Electron corporation model Nexus 670 spectrophotometer. The ^{1}H NMR and ^{13}C NMR analyses were recorded in $CDCl_3$ and d6 - DMSO as solvents, respectively on a Bruker 400 spectrometer. MALDI MASS was recorded using Matrix Assisted Laser Desorption Time of Flight Mass Spectrometer. A Netzsch DSC-200 differential scanning calorimeter was used for the calorimetric analysis at a heating rate of 10 °C /min under continuous flow of nitrogen and TGA analysis was carried out using TGA 2950 from TA Instruments. The dielectric constant (DC) of the prepared composites were determined with the help of an impedance analyzer (Solartron impedance/gain phase analyzer 1260) using Pt electrode at 40 °C in a frequency range of 1 MHz. Powder X-ray diffraction patterns (XRD) were verified on Rigaku Mini flex diffractometer with Cu-KR radiation. A JEOL JSM-6360 field emission scanning electron microscope was utilized to analyze the morphologies of the prepared samples. HR-TEM (JEM-3010, JEOL, Tokyo, Japan) was used to study the phase morphology of nanocomposites, which was operated at 80 kV with a measured point-to-point resolution of 0.23 Nm. Anti microbial activities has been studied by well-diffusion methods for two gram positive and gram negative bacteria.

Results and discussion

Raman, FTIR and XRD spectra of GO and functionalized GO reinforcement

XRD analysis was carried out to confirm the formation of graphene oxide (GO) from graphite (Fig. 1). The formation of graphene oxide (GO) was confirmed by the formation of a new peak characteristic of (002) plane at an angle of 26.52° and the disappearance of peak around 11.0° [39]. Further, the oxidation of graphite is evidenced from the increase in interlayer distance d-spacing from 3.6 to 8.6° for GO.

Raman spectroscopy was used to identify the structural changes of amine functionalized graphene oxide from graphene oxide material. Raman spectra of graphene oxide (GO) and paraphenylene diamine functionalized graphene oxide (*f*-GO) were shown in Fig. 2(a). In both spectra, the peak around 1600 cm^{-1} represents a graphitic peak known as G-band and the peak near 1340 cm^{-1} indicates D band, respectively. The presence of D band was the evident for the disorder in the graphene oxide, which is caused by the functionalization of graphite material. The growth band (G-band) arouse due to the in-plane vibration modes of sp^2 hybridized carbon – carbon bonds in the graphene oxide material [40, 41].

The FTIR spectra of graphene oxide and paraphenylene diamine functionalized graphene oxide are shown in Fig. 2(b). The absorption peaks appeared at 3425 and

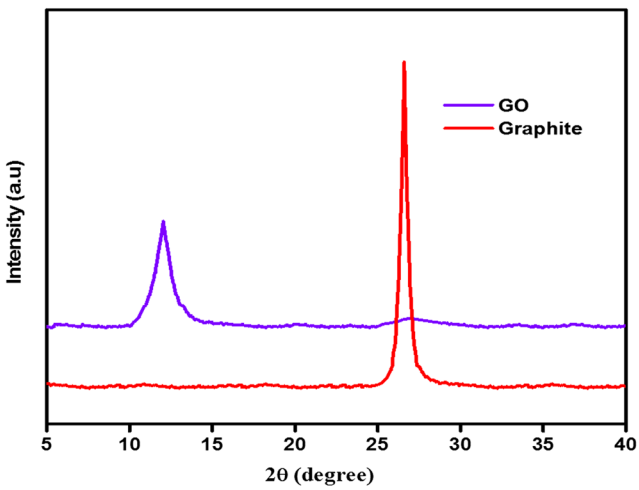

Fig. 1 XRD pattern of graphite and graphene oxide (GO) powder

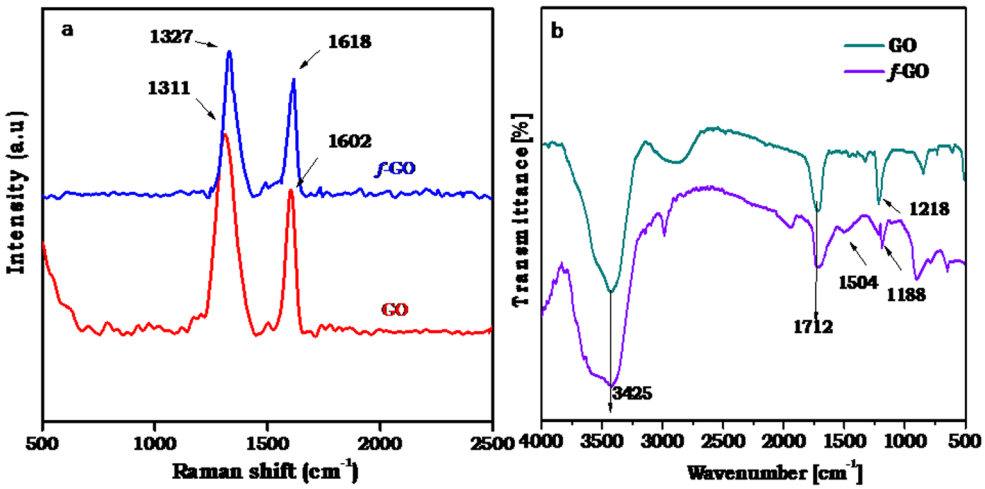

Fig. 2 The Raman (a) and FT-IR (b) spectra of graphene oxide and functionalized graphene oxide

1712 cm^{-1} indicate the presence of–OH and –CO in –COOH groups (GO). The absorption peak present at 1218 cm^{-1} authenticates the presence of epoxide linkage and its high intensity gives the information about the ring opening reaction which occurs through epoxide linkage in GO during the functionalization process. In addition, the graphene oxide is getting reduced by paraphenylene diamine during the functionalization process [42]. In the IR spectra of *f*-GO, the presence of C–N bond stretching vibration at 1504 cm^{-1} indicates the formation of new bond between the carbon atoms of GO and nitrogen atoms of PPDA. The peak appeared at 1188 cm^{-1} is attributed to the asymmetric stretching of C-N-C bond [43]. Further, the stretching frequency at 1504 cm^{-1} was also observed from the PPDA, which is attached to the basal plane of GO due to pi-pi interaction between GO and PPDA compound [44].

FTIR studies

FTIR spectra of cardanol based aliphatic ether linked benzoxazine ($CBAE_2Bz$, $CBAE_4Bz$ and $CBAE_8Bz$)

The structure of aliphatic ether linked cardanol based benzoxazine ($CBAE_nBz$) monomer was confirmed by FTIR, ^{1}H-NMR and ^{13}C–NMR spectroscopy. Fig. 3 shows the FTIR spectrum of aliphatic ether linked cardanol based benzoxazine $CBAE_2Bz$ monomer.

FTIR spectrum of $CBAE_2Bz$ shows the absorption peak appeared at 3009 cm^{-1} is due to C–H aromatic stretching vibrations. The peaks absorption appeared at 2923 and 2854 cm^{-1} were assigned to aliphatic C–H bond in $CBAE_2Bz$ monomer. The formation of oxazine ring was evidenced by the appearance of peak at 951 cm^{-1}, which corresponds to O–CH_2–N and the characteristic absorption peaks appeared at 1627 and 1512 cm^{-1} are corresponding to 1,2,3-trisubstituted benzene [45]. The asymmetric and symmetric stretching vibrations of Ar-O-C are evidenced by the peaks at 1241 and 1031 cm^{-1}, respectively. The peak present at 1375 cm^{-1} is assigned to CH_2 wagging of oxazine ring [43]. Further, the FTIR spectra of $CBAE_4Bz$ and $CBAE_8Bz$ monomers (SI) are also showing similar type absorption peaks, which are confirming the formation of aliphatic ether linked cardanol based benzoxazine ($CBAE_nBz$) monomers.

FTIR spectra of various weight percentage of *f*-GO incorporated $PCBAE_2Bz$ composites

The cardanol based aliphatic ether linked benzoxazine polymer ($PCBAE_2Bz$) and various weight percentages of *f*-GO reinforced cardanol based aliphatic ether linked benzoxazine (*f*-GO((1,3 and 5 wt.%)/$PCBAE_2Bz$) composites show an absorption peak at 1455 cm^{-1} indicates the presence of tetra substituted benzene ring (Fig. 4), which are confirming the ring-opening polymerization of aliphatic ether linked cardanol

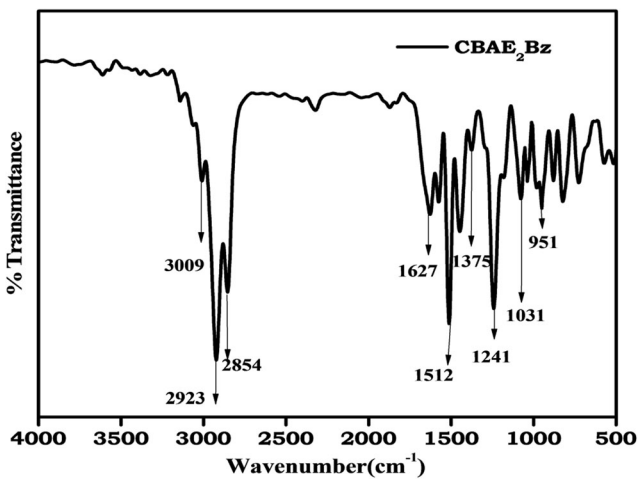

Fig. 3 FTIR spectrum of aliphatic ether linked cardanol based benzoxazine $CBAE_2Bz$

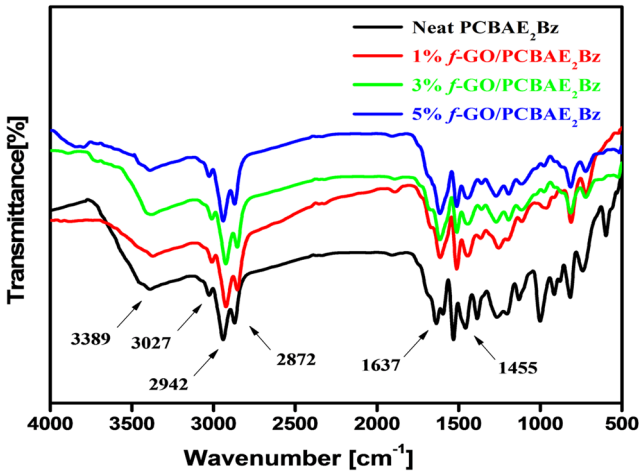

Fig. 4 FTIR spectra of neat $PCBAE_2Bz$ and various weight percentage of *f*-GO (1,3,5%) incorporated composites

based benzoxazine ($CBAE_2Bz$) monomer. The absorption peaks noticed at 2942 cm^{-1} and 2872 cm^{-1} indicate the presence of C–H aliphatic groups. The presence of aromatic C–H stretching was confirmed by the absorption peak observed at 3027 cm^{-1}. The absorption peak appeared at 1637 cm^{-1} was ascribed to aliphatic C = C stretching frequency. The broad peak noticed at 3389 cm^{-1} is corresponding to the vibration of O–H linkage of phenolic group present in $PCBAE_2Bz$. Further, *f*-GO(1, 3 and 5 wt.%)/$PCBAE_2Bz$ composites show a small shift and broadening of these peaks with respect to the varying weight percentage of *f*-GO. The cardanol based aliphatic ether linked benzoxazine polymers like $PCBAE_4Bz$ and $PCBAE_8Bz$ and their respective *f*-GO reinforced composites also show similar patterns of IR spectra (SI).

NMR studies of cardanol based aliphatic ether linked benzoxazine $CBAE_2Bz$ monomer

^{1}H NMR spectra of $CBAE_2Bz$ monomer

The ^{1}H NMR spectrum of aliphatic ether linked cardanol based benzoxazine monomer ($CBAE_2Bz$) is shown in Fig. 5. The peak observed at 0.85 ppm (a) is due to $–CH_3$ protons. The peaks corresponding to aliphatic CH_2 protons were appeared at 1.29, 1.30 and 1.58 ppm (b, c and d). The peak visualized at 2.15 ppm (e) is corresponding to the protons that are adjacent to double bond ($-CH_2-CH=$). The peak noticed at 2.62 ppm (f) is ascribed to $-CH_2Ar$ protons. The peak appeared at 4.55 ppm (g) is due to $–CH_2-O-Ar$ protons and the peak emerged at 4.618 ppm (h) is assigned to $Ar-CH_2-N$ protons. The peak observed at 5.51 ppm (j) is allocated to -CH=CH- protons present in the long alkyl side chain of monomer. The peak appeared at 5.31 ppm (i) is consigned to $–O-CH_2N$ protons. The peaks noted between 6.54 and 7.07 ppm (k-o) confirm the presence of aromatic protons. Similar types of NMR spectra were received for $CBAE_4Bz$ and $CBAE_8Bz$ monomers (SI).

^{13}C NMR spectra of $CBAE_2Bz$ monomer

The formation of $CBAE_2Bz$ monomer was also characterized by ^{13}C NMR (Fig. 6). The peaks appeared at 14.26 ppm and 36.66 ppm confirm the presence of aliphatic carbon atoms(a). The peaks corresponding to ph-CH_2-N, -O-CH_2-CH_2-O- and -O-CH_2-N carbons were observed at 58.48 ppm (b), 70.40 ppm and 89.32 ppm(d), respectively. These results substantiate the oxazine ring formation along with aliphatic ether linkage bonding. The

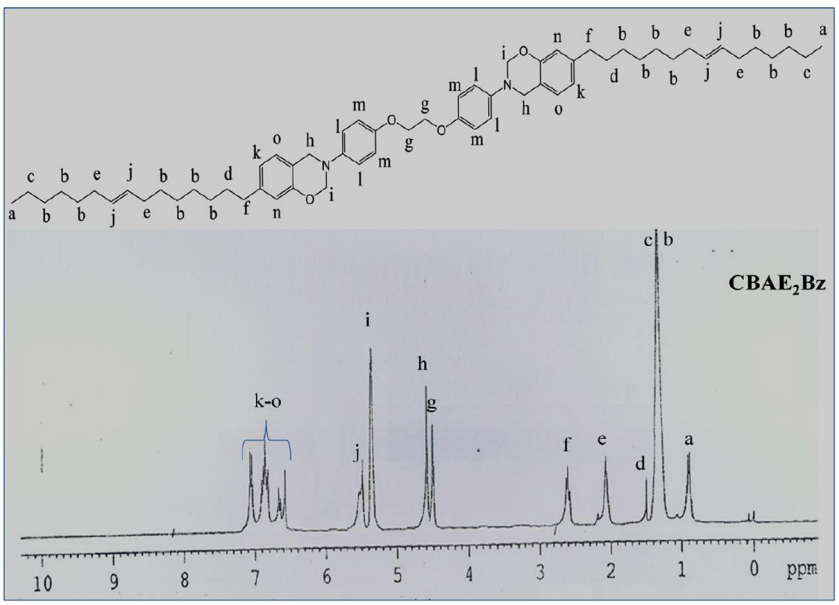

Fig. 5 ^{1}H NMR spectrum of cardanol based aliphatic ether linked benzoxazine ($CBAE_2Bz$) monomer

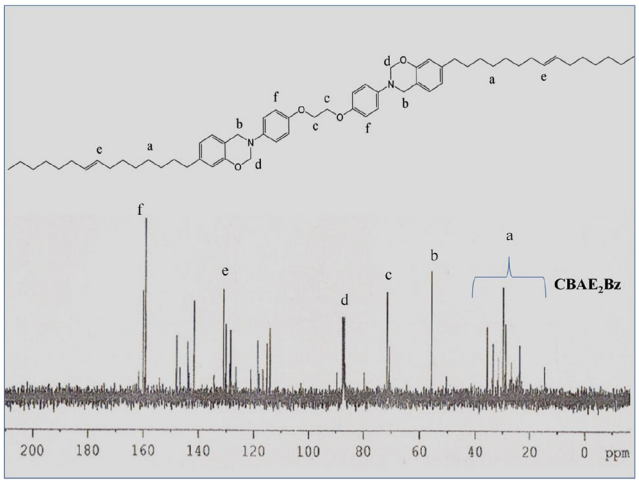

Fig. 6 ^{13}C NMR spectrum of cardanol based aliphatic ether linked benzoxazine ($CBAE_2Bz$) monomer

peak appeared at 129.34(e) ppm confirms the aliphatic -C=C- carbon present in the side chain of the cardanol. The peaks observed at 159.50 ppm and 160.50 ppm (f) were assigned to aromatic carbon atoms. The $CBAE_4Bz$ and $CBAE_8Bz$ monomers also exhibit similar type of ^{13}C NMR spectra (SI).

MALDI-mass analysis

MALDI-Mass is an imperative technique used to determine the higher molecular weight organic molecules like proteins, polymers, etc. The formation of cardanol based aliphatic ether linked benzoxazine monomers can also be confirmed by MALDI Mass spectroscopy and among the three monomers MALDI mass spectra was taken only for $CBAE_2Bz$. The MALDI-Mass result (Fig. 7) substantiates the molecular weight of aliphatic ether linked benzoxazine monomer ($CBAE_2Bz$) as 896.28, which is in good agreement with the theoretically calculated value of molecular weight. Thus, the formation of cardanol based aliphatic ether linked benzoxazine monomer ($CBAE_2Bz$) is inferred from the data resulted from ^{1}H NMR, ^{13}C NMR, MALDI Mass and FTIR analysis.

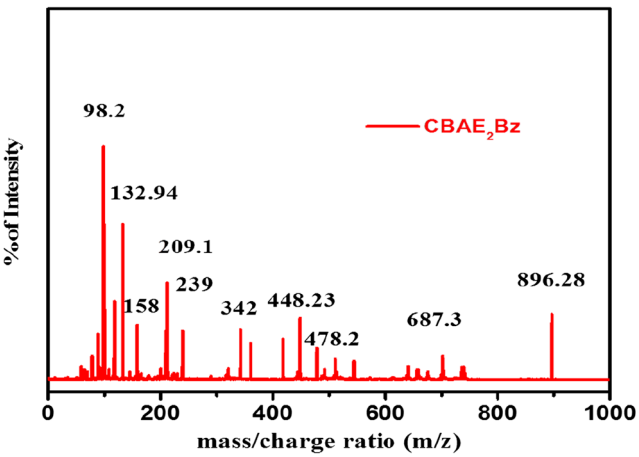

Fig. 7 MALDI-Mass spectrum of cardanol based aliphatic ether linked benzoxazine ($CBAE_2Bz$) monomer

Differential scanning calorimetry (DSC)

DSC analysis was carried out to ascertain the curing behavior of monomers like $CBAE_2Bz$, $CBAE_4Bz$ and $CBAE_8Bz$ and these monomers differ only in aliphatic ether chain length. Figure 8 shows the DSC thermogram of $CBAE_2Bz$, monomer. DSC thermograms of all the three monomers show similar curing behavior and exhibits single exothermic peak.

The onset curing temperature, melting temperature and peak temperature were found to be decreasing with respect to the increasing chain length ($CBAE_2Bz > CBAE_4Bz > CBAE_8Bz$) of the monomers and the values are presented in Table 1. The presence of aliphatic ether substituent in benzoxazine plays a vital role in ring opening polymerization. Benzoxazine with short chain or withdrawing groups are showing an exothermic peak at higher temperature, while benzoxazine with longer chain length or more electron donating ether linkage shows an exothermic peak at lower temperature. Hence, all the three benzoxazine monomers have electron donating ether linkages and thus ring opening polymerization occurs relatively at lower temperature. Further, the large difference between melting temperature and onset curing temperature of these monomers infer their good processing behavior.

DSC analysis was also carried out for *f*-GO incorporated $PCBAE_nBz$ ($n = 2$, 4 and 8) polymers (Table 2) (*f*-GO/$PCBAE_2Bz$). From the data, it is clear that the Tg values of the prepared polybenzoxazine matrices are decreasing with increase in chain length of aliphatic ether. After the incorporation of *f*-GO, the Tg values were found to be increasing as shown in Table 2. The restricted motion of bulky polybenzoxazine molecular chains and the incorporation of amine functionalized *f*-GO impart further more rigidity, which is responsible for the improved Tg values for *f*-GO incorporated $PCBAE_nBz$ composites.

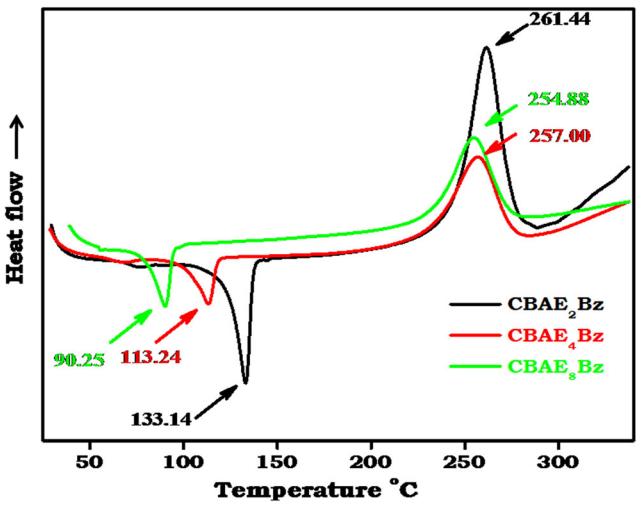

Fig. 8 DSC graphs of $CBAE_2Bz$, $CBAE_4Bz$ and $CBAE_8Bz$ monomers

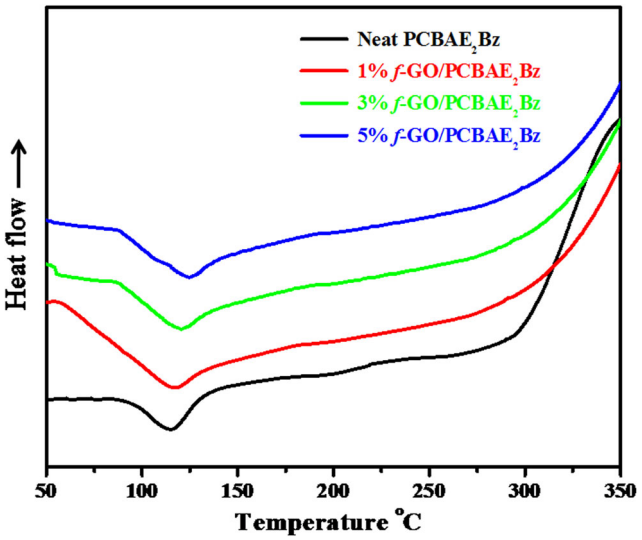

Fig. 9 DSC graphs of neat $PCBAE_2Bz$ and various weight percentage of *f*-GO incorporated $PCBAE_2Bz$ composites

Among the three composites, the *f*-GO/$PCBAE_2Bz$ shows higher Tg value when compared to that of the *f*-GO/$PCBAE_4Bz$ and *f*-GO/$PCBAE_8Bz$ composites (Table 2). As alkoxy chain length decreases, the Tg value increase in the case of polybenzoxazine polymers, however, the incorporation of *f*-GO in all the three polymer matrices leads to an increase in Tg values. This is due to interlocking effect of amine functionalized GO, which hinders the segmental motions of polymer chains (Fig. 9). The increase of Tg values with increasing the content of *f*-GO in the prepared polymer matrix might be also due to increasing number of hydrogen bonding with increasing quantity of *f*-GO compound and improved cross- link density of the prepared composites. Further, the hydrogen bonding may be occurred between two hydroxyl groups of GO and polybenzoxazine, the carbonyl group of GO and hydroxyl group of polybenzoxazine, and hydroxyl group of GO and nitrogen atom on the Mannich bridge of polybenzoxazine [46]. Thus, the improved Tg values were noticed all the three systems with the incorporation of increasing quantity of f-GO in the prepared composites (Table 2).

Thermo gravimetric analysis (TGA)

The influence of *f*-GO content on the thermal stability of *f*-GO incorporated $PCBAE_nBz$ (n = 2, 4 and 8) composites were analyzed by TGA and the thermogram of *f*-GO/$PCBAE_2Bz$ is shown in Fig. 10. The TGA results infer that the thermal stability of $PCBAE_8Bz$ polymer is lower than that of the $PCBAE_4Bz$ and $PCBAE_2Bz$ polymers (SI). This is because of an increase of aliphatic alkoxy chain length, which is flexible and may get fragmented easily from the polymer chain when compared to that of polymer with lower length of aliphatic chains. The value of char yield also decreases with increase in aliphatic ether linkage.

The char yields of $PCBAE_2Bz$, $PCBAE_4Bz$ and $PCBAE_8Bz$ polymers are 18.7, 16.4 and 15.2% respectively. However, the

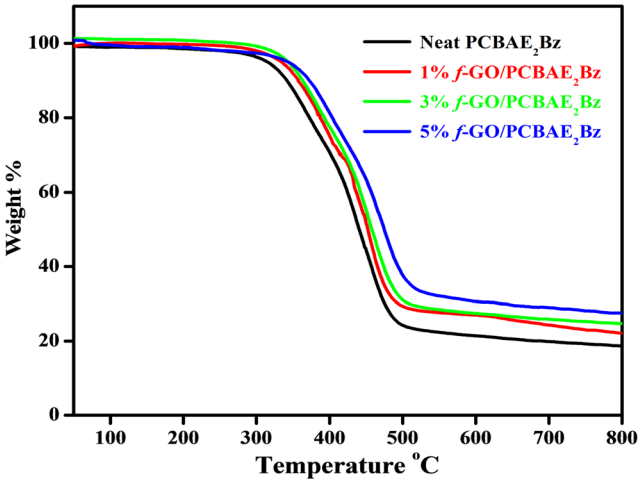

Fig. 10 TGA thermograms of $PCBAE_2Bz$ and various weight percentage of *f*-GO incorporated $PCBAE_2Bz$ composites

char yields of the composites were increased with increasing weight percentages of *f*-GO. This may be due to the introduction of graphene oxide and the presence of aromatic ring from paraphenylene diamine in the polymer matrix, which act as physical barrier during thermal decomposition and in turn results higher char yield (Table 2). The 30% weight loss was observed at 402 °C, 394 °C and 392 °C for $PCBAE_2Bz$, $PCBAE_4Bz$ and $PCBAE_8Bz$ polybenzoxazines, respectively (Table 2). From the values of weight loss (Table 2) observed, it is inferred that the alkoxy chain length greatly influences thermal stability and char yield of the composite materials.

Dielectric properties

The dielectric properties of aliphatic ether linked cardanol based polybenzoxazines ($PCBAE_2Bz$) and various weight percentages of *f*-GO/$PCBAE_2Bz$ composites were studied and the results obtained are presented in Fig. 11. The results

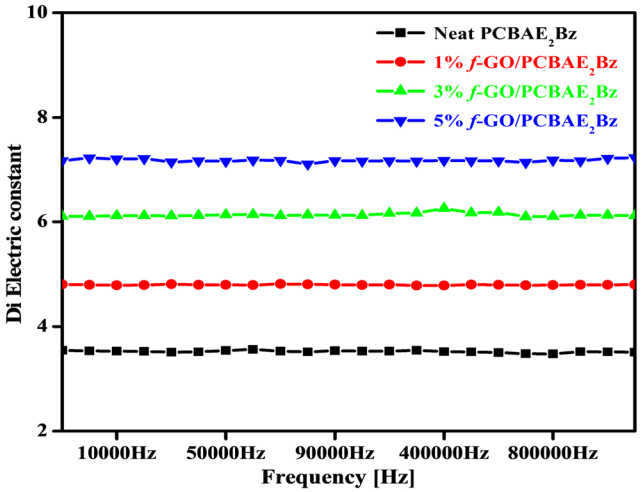

Fig. 11 Dielectric constant of $PCBAE_2Bz$ and various weight percentage of *f*-GO incorporated $PCBAE_2Bz$ composites

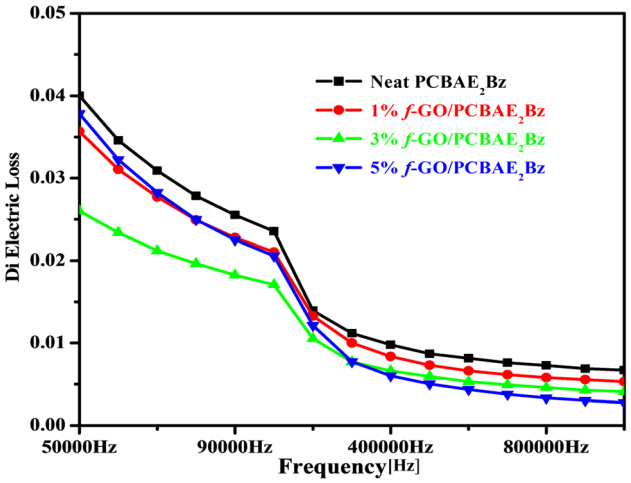

Fig. 12 Dielectric loss of $PCBAE_2Bz$ and various weight percentages of *f*-GO/$PCBAE_2Bz$ composites

were compared with that of the *f*-GO/$PCBAE_4Bz$ and *f*-GO/$PCBAE_8Bz$ composites (SI). The dielectric constant values were found to be increased with increase in the concentration of *f*-GO. The dielectric value of $PCBAE_2Bz$, $PCBAE_4Bz$ and $PCBAE_8Bz$ polymer matrices are 3.51, 3.39 and 3.28 respectively, where as that of 1 wt.% *f*-GO/PCBAEnBz composites are 4.79, 4.59 and 4.39 respectively.

The increase in dielectric values are due to the presence of the conductive nature of the functionalized graphene oxide in the polymer composites. The conductivity of the composites increases as charge carriers increases at the interface between polybenzoxazine and *f*-GO. In addition to that the increase in the value of dielectric constant may also be due to the movement of free charge carriers within the polymer matrix [47]. The amine functionalization may also partially to reduce the GO, which results an enhanced dielectric constant [48]. Hence, the *f*-GO reinforcement in the polymer matrix is expected to cause in-situ reduction and thereby forms a conducting network, which results the formation of high k composites [49]. The good dispersion of GO in the polymer matrix, which is aided by amine functionalization and the chemical compatibility of *f*-GO with aliphatic ether linked polybenzoxazine matrix also contributed to increase the value of dielectric constant.

The incorporation of *f*-GO results in decreased dielectric loss for *f*-GO/$PCBAE_2Bz$ composites as shown in Fig. 12. The amine functionalized GO provides bonding sites for polybenzoxazine matrix, which restricts the movement of the molecular dipoles, improves the dispersion and enhances the interfacial adhesion between *f*-GO and $PCBAE_2Bz$ polymers [50]. The *f*-GO/$PCBAE_4Bz$ and *f*-GO/$PCBAE_8Bz$ composites also exhibit similar kind of dielectric loss and make suitable for dielectric application related to the high k value (SI).

Morphological properties of *f*-GO/$PCBAE_nBz$ nanocomposites

The distribution of varying weight percentage of *f*-GO in the aliphatic ether linked cardanol based polybenzoxazine matrix phase was studied using SEM. The SEM image (Fig. 13) of polybenzoxazines synthesized from cardanol showed uniform and smooth surfaces. After the incorporation of *f*-GO reinforcement, the SEM images become the network and wrinkled structure without much agglomeration. The wrinkled structure is due to the presence of amine terminated graphene oxide in the composites, which is expected to improve Tg and thermal stability of the prepared composites. In addition, a new type of homogeneous distribution of GO is favored by paraphenylene diamine group functionalization. The high reactivity of

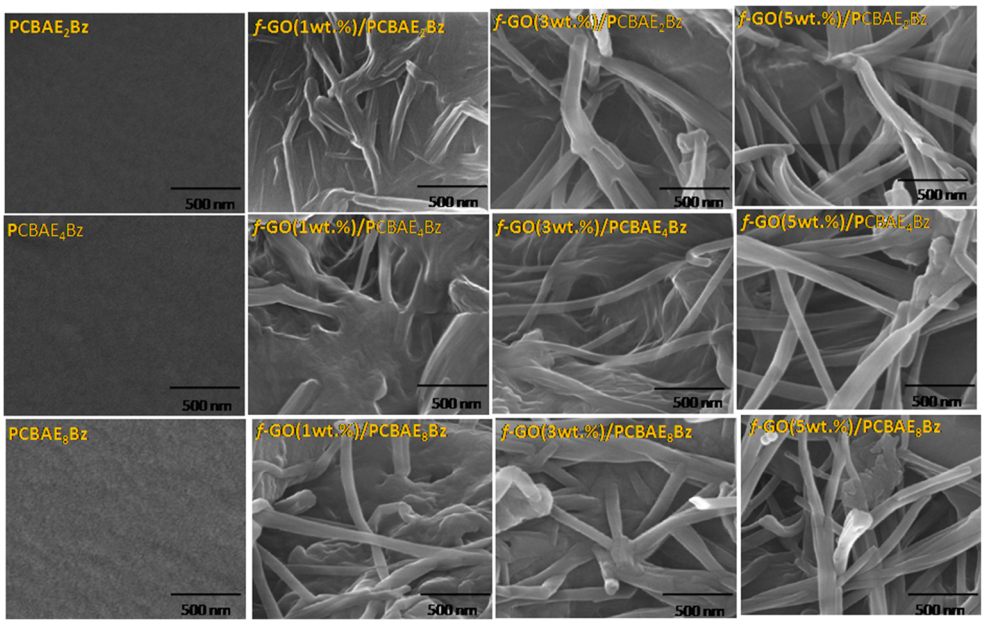

Fig. 13 SEM images of $PCBAE_nBz$ and various weight percentages of *f*-GO/$PCBAE_nBz$ composites

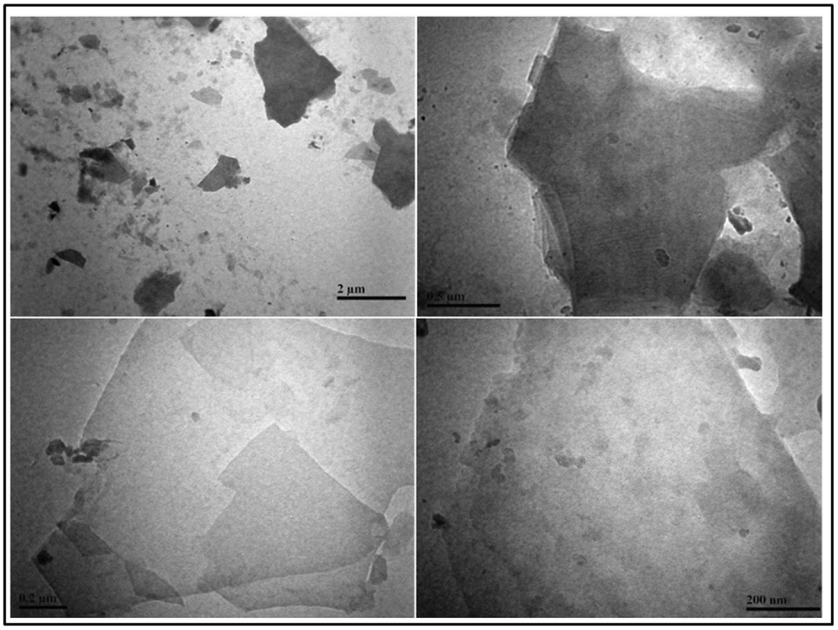

Fig. 14 TEM images of 3 wt.% *f*-GO/PCBAE$_2$Bz composite at different magnifications

epoxide group of GO with amine group increases the interfacial adhesion without the aid of any catalyst, which results in homogeneous dispersion [51, 52]. Further, the TEM images (Fig. 14) confirm the uniform and the single sheet layer graphene oxide distribution in the aliphatic ether linked cardanol based polybenzoxazine (3%*f*-GO/PCBAE$_2$Bz) composites.

XRD studies of neat PCBAE$_2$Bz matrix and *f*-GO/PCBAE$_2$Bz composites

The XRD patterns of all the composites of *f*-GO/PCBAE$_2$Bz shows (Fig. 15) a broad amorphous peak at 2θ = 18.4, which indicates the homogeneous dispersion of amine functionalized graphene oxide molecules and the formation of stable composites with polybenzoxazine matrices through covalent bonding.

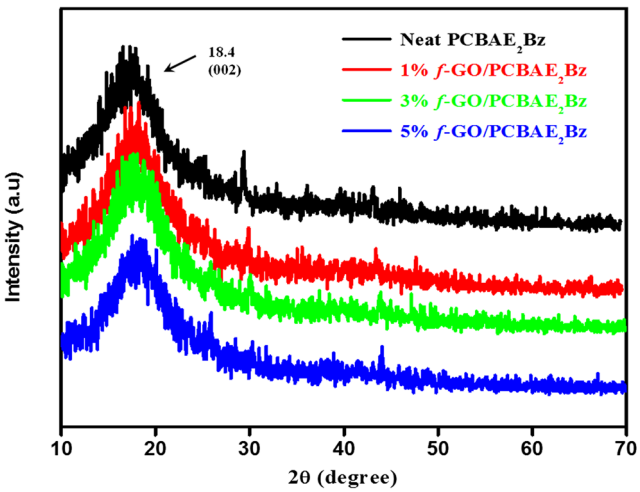

Fig. 15 XRD of neat PCBAE$_2$Bz and *f*-GO(1,3&5 wt%)/PCBAE$_2$Bz composites

Anti microbial activity by well-diffusion methods

Among the *f*-GO/PCBAE$_n$Bz (*n* = 2, 4, and 8**)** systems, *f*-GO/PCBAE$_2$Bz system shows higher thermal stability and lower value of dielectric constant and hence, antimicrobial studies were carried out for this composites (Fig. 16).

The results of antimicrobial activity by well diffusion method are presented in Table 3. As shown in Table 3, PCBAE$_2$Bz matrix sample and varying weight percentages of *f*-GO/PCBAE$_2$Bz composites show good antibacterial activity. From zone of inhibition (ZOI) values, it is clear that the zone of inhibition increases with increase in weight percentage of *f*-GO, which is also ascertain that *f*-GO/PCBAE$_2$Bz possesses an increased toxicity against *Bacillus subtilis, Staphylococcus aureus, Pseudomonas aeruginosa* and *Escherichia coli* bacteria with respect to the weight percentage content of graphene oxide. The minimum inhibitory concentration (MIC) values were also determined and is given in Table 3. From the MIC values, it was found that the PCBAE$_2$Bz is active for *Pseudomonas aeruginosa* only at 50 μg/mL. Further, the antimicrobial activity is also tested at the lowest concentration and their results conclude that there is no significant inhibition zone for PCBAE$_2$Bz against the pathogens like *Bacillus subtilis, Staphylococcus aureus, Pseudomonas aeruginosa* and *Escherichia coli* at 6.25 μg/mL. However, the average ZOI for 1 wt% *f*-GO/PCBAE$_2$Bz composites at a concentration of 6.25 μg/mL are 11 mm, 16 mm, 0 mm and 12 mm for *Bacillus subtilis, Staphylococcus aureus, Pseudomonas aeruginosa and Escherichia coli* bacteria, respectively.

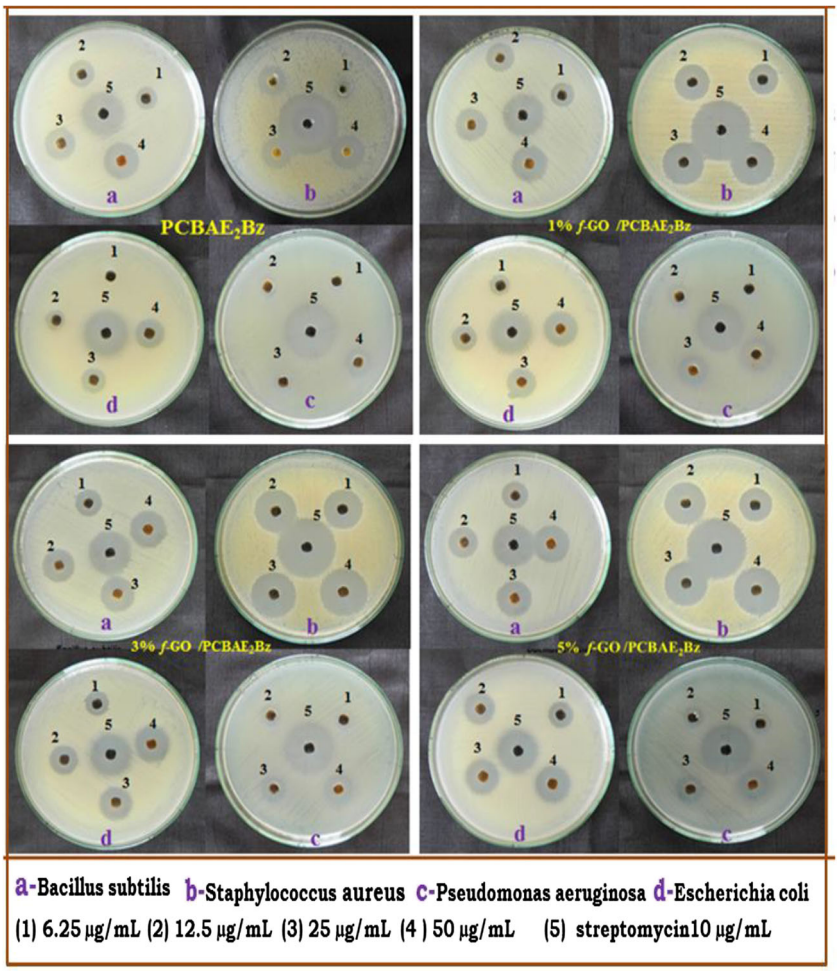

Fig. 16 Antimicrobial activity by well diffusion method of $PCBAE_2Bz$ and *f*-GO (1,3 and 5 wt%)/$PCBAE_2Bz$ composites system

When the weight percentage of *f*-GO was increased to 3 wt%, the zone of inhibitions at 6.25 µg/mL, are 12 mm, 17 mm, 10 mm and 14 mm. respectively. The incorporation of 5 wt.% *f*-GO shows similar zone of inhibition except for *Pseudomonas aeruginosa* as 13 mm,17 mm,11 mm,14 mm respectively. However, the polymer matrix as well as all the composites show potential activity against all the pathogens at 50 µg/mL. It is assumed that the antimicrobial activity of neat $PCBAE_2Bz$ and *f*-GO/$PCBAE_2Bz$ composites may be due to cellular damage of bacterial cell by either generation of reactive oxygen species or physical disruption [52]. Since, $PCBAE_2Bz$ and *f*-GO/$PCBAE_2Bz$ composites show toxicity against bacteria, it can also be concluded that all the other systems like $PCBAE_4Bz$ and *f*-GO/$PCBAE_4Bz$ and $PCBAE_8Bz$ and *f*-GO/ $PCBAE_8Bz$ are also expected to have antimicrobial property according to their molecular structure and weight percentage content of *f*-GO.

Z–scan measurements

A 635 nm continuous wave (CW) diode laser with 5 mW power was used to perform the Z–scan measurements. The $PCBAE_2Bz$ and (1, 3 and 5 wt.%) *f*-GO/$PCBAE_2Bz$ composites in organic solvent were kept in a 1 mm thick cuvette and it was placed in the laser beam propagation direction. The approximate concentration of the samples has been made for the present experimental studies in such a case that the measured Rayleigh length ($Z_R = 1.4$ mm) has to be greater than the sample length (L). For the closed aperture Z–scan measurements, an iris shaped aperture is placed in front of the detector and the corresponding change in the transmittances are measured using digital optical power meter. In open aperture Z–scan method, the aperture is removed and the entire beam transmittance through the sample is collected by a suitable lens.

From the open aperture and closed aperture Z–scan measurement, the nonlinear absorption coefficient (β) and nonlinear index refraction (n_2) of $PCBAE_2Bz$ matrix and 1, 3 and 5 wt.% of *f*-GO incorporated $PCBAE_2Bz$ composites in chloroform were measured. The solutions of $PCBAE_2Bz$ matrix and 1, 3 and 5 wt.% of *f*-GO incorporated $PCBAE_2Bz$ samples are mounted on the micrometer and progressively translated along the Z-direction. When the sample was moved from negative Z in to focus (Z = 0), the

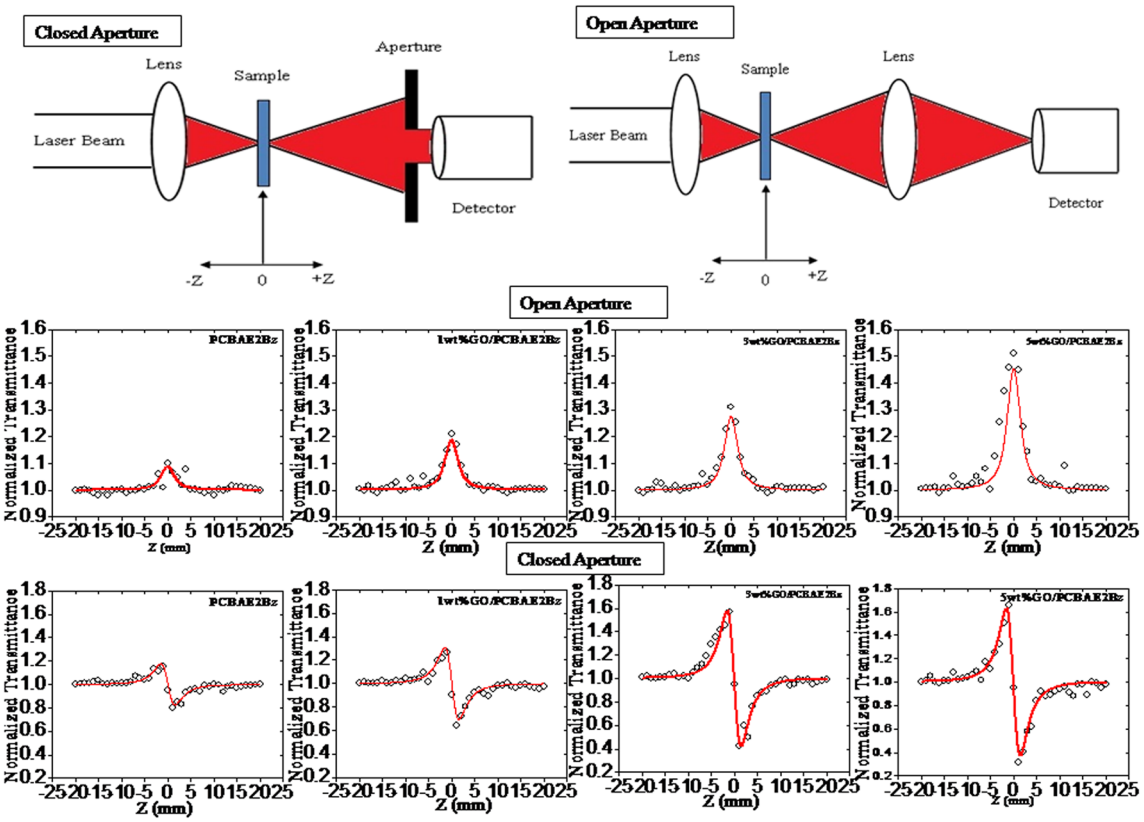

Fig. 17 Closed aperture and open aperture Z-scan arrangements, open and closed aperture Z–scan curves of $PCBAE_2Bz$ matrix *and GO*/$PCBAE_2Bz$ composites

beam intensity become low that indicates the occurrence of negligible non-linear refraction and this result confirms the transmittance of the sample is comparatively constant. As the sample is brought closer to the focus (Z = 0), the beam intensity increases, which is leading to self-lensing in the sample. When the test sample is moved away from focus i.e., positive Z, the beam divergence causes decrease in transmittance at the aperture. The closed aperture Z–scan data is divided by the corresponding open aperture Z–scan data, to separate the non-linear refraction (NLR) component from non-linear absorption (NLA), which then reflects the pure non-linear refraction of the sample [53, 54]. The measured pure non-linear refraction Z–scan curves for different weight percentage GO doped bio-resource based polybenzoxazine matrix are shown in Fig. 17. The observed normalized transmittance in the prepared polymer and its composites exhibit a pre-focal peak followed by a post-focal valley signature indicating self-defocusing or negative nonlinear refraction. This self-defocusing effect of the samples might be due to induced thermal nonlinearity mechanism resulted from continuous absorption of laser radiation by the samples at 635 nm. In addition, it is also observed from the Fig. 17. That the peak-valley separation was also increased with respect to the incorporation of GO to $PCBAE_2Bz$ matrix. The physical origin of non-linear refractions may be due to any one of the reasons like electronic transition, molecular transition, electrostatic or thermal conversion in nature [55]. The closed aperture Z–scan curve for all samples show a peak–valley separation of ~5 Z_R. A peak-valley separation of the sample is more than 1.7 times of the Rayleigh range (Z_R), which is clearly indicating the kind of thermal nonlinearity under CW regime and this confirms the observed NLO response of $PCBAE_2Bz$ matrix and its composites are third-order process [56].

Table 1 Characteristic parameters of $CBAE_2Bz$, $CBAE_4Bz$ and $CBAE_8Bz$ monomers

	Melting temp(°C)	Onset temp(°C)	Peak temp(°C)	End temp(°C)	Exothermic enthalpy(J/g)
$CBAE_2Bz$	133.1	228.6	261.4	287.9	89.7
$CBAE_4Bz$	113.2	212.5	257.0	284.4	52.4
$CBAE_8Bz$	90.2	209.0	254.8	283.8	47.2

Table 2 Characteristic parameters obtained from TGA, DSC and Dielectric Analysis of various weight percentages of *f*-GO incorporated $PCBAE_nBz$ composites

S.No.		T_g (°C)	10%Wt.loss (°C)	20%Wt.losss (°C)	30%Wt.loss (°C)	Char yield % (800 °C)	Dielectric Constant at 1 MHz
1	**$PCBAE_2Bz$ matrix**	114.3	341	372	402	18.7	3.5
2	1Wt.% *f*-GO/$PCBAE_2Bz$	117.1	357	387	416	22.1	4.8
3	3Wt.% *f*-GO/$PCBAE_2Bz$	120.5	363	392	416	24.6	6.1
4	5Wt.% *f*-GO/$PCBAE_2Bz$	124.6	372	404	433	27.5	7.2
5	**$PCBAE_4Bz$ matrix**	108.3	335	365	394	16.4	3.4
6	1Wt.% *f*-GO/$PCBAE_4Bz$	112.6	341	373	402	19.3	4.6
7	3Wt.% *f*-GO/$PCBAE_4Bz$	116.5	350	381	410	21.4	6.0
8	5Wt.% *f*-GO/$PCBAE_4Bz$	118.1	359	390	419	23.6	6.8
9	**$PCBAE_8Bz$ matrix**	98.2	330	364	392	15.2	3.2
10	1Wt.% *f*-GO/$PCBAE_8Bz$	100.8	338	369	395	17.3	4.34
11	3Wt.% *f*-GO/$PCBAE_8Bz$	104.4	345	376	405	19.5	4.98
12	5Wt.% *f*-GO/$PCBAE_8Bz$	106.1	353	382	411	21.6	6.21

The quantity ΔT_{p-v} is the difference between the normalized peak and valley transmittances, and represented by,

$$\Delta T_{P-V} = 0.406(1-S)^{0.25}|\Delta\varphi_0| \quad (1)$$

where $|\Delta\varphi_0|$ is the axis phase shift at the focus, $S = 1-\exp(-2r_0^2/\omega_0^2)$ is the aperture linear transmittance, here r_0 = aperture radius and ω_0 = beam radius at the aperture in the linear regime. The value of n_2 of the sample is given by,

$$n_2 = \frac{\Delta\varphi_0\lambda}{2\pi I_0 L_{eff}}\left(\frac{cm^2}{W}\right) \quad (2)$$

Here I_0 = laser input intensity, λ = laser wavelength, and L_{eff} = effective sample thickness.

T The open aperture Z–scan curves are obtained for all the samples and they exhibit a maximum transmittance at the focus (Fig. 17). When the quantity GO sample increases in the polymer sample, the transmittance at the focus is also increases and this is the characteristic signature of saturable absorption (SA). The magnitude of β can be calculated using the relation,

$$\beta = \frac{2\sqrt{2}\Delta T}{I_0 L_{eff}}\left(\frac{cm}{W}\right) \quad (3)$$

The magnitude of third-order nonlinear susceptibility $\chi^{(3)}$ could be measured using the following relations,

$$Re\left[\chi^{(3)}\right](esu) = 10^{-4}\frac{\varepsilon_0 c^2 n_0^2}{\pi} n_2\left(\frac{cm^2}{W}\right) \quad (4)$$

$$Im\left[\chi^{(3)}\right](esu) = 10^{-2}\frac{\varepsilon_0 c^2 n_0 \lambda}{4\pi}\beta\left(\frac{cm}{W}\right) \quad (5)$$

$$\chi^{(3)} = \left[\left(Re\left(\chi^{(3)}\right)\right)^2 + \left(Im\left(\chi^{(3)}\right)\right)^2\right]^{\frac{1}{2}} \quad (6)$$

where ε_0 = vacuum permittivity and c = light velocity in vacuum. Systematic measurements were performed to study the

Table 3 Results of anti-bacterial activity of $PCBAE_2Bz$ and *f*-GO (1,3 and 5 wt%)/$PCBAE_2Bz$ composites

Sample Code	Zone of inhibition (mm) and MIC (μg/mL)															
	Bacillus subtilis				*Staphylococcus aureus*				*Pseudomonas aeruginosa*				*Escherichia coli*			
	6.25 μg	12.5 μg	25 μg	50 μg	6.25 μg	12.5 μg	25 μg	50 μg	6.25 μg	12.5 μg	25 μg	50 μg	6.25 μg	12.5 μg	25 μg	50 μg
$PCBAE_2Bz$ matrix	–	10	13	15	9	14	18	22	–	–	–	13	10	13	15	18
1wt.%f-GO/$PCBAE_2Bz$	11	14	16	18	16	18	22	23	–	11	13	15	12	15	16	19
3wt.%f-GO/$PCBAE_2Bz$	12	15	16	18	17	20	23	24	10	12	13	15	14	16	18	20
5wt.%f-GO/$PCBAE_2Bz$	13	15	17	19	17	21	23	25	11	12	15	17	14	16	19	20
streptomycin (10 μg/mL)	22				30				24				21			

- = Not active.

Table 4 : Third-order NLO properties of $PCBAE_2Bz$ and GO/$PCBAE_2Bz$ samples

Sample (wt%)	n_2 X 10^{-6} (cm^2/W)	β X 10^{-2} (cm/W)	Re (χ^3) X 10^{-5} (esu)	Re (χ^3) X 10^{-5} (esu)	χ^3 X 10^{-4} (esu)
$PCBAE_2Bz$ matrix	−0.74	−1.26	−3.89	−0.33	0.39
1wt.%GO/$PCBAE_2Bz$	−1.08	−1.33	−5.68	−0.35	0.56
3wt.%GO/$PCBAE_2Bz$	−1.73	−4.69	−9.09	−1.25	0.91
5wt.%GO/$PCBAE_2Bz$	−1.93	−7.93	−10.15	−2.10	1.03

influence on the magnitudes of n_2 and β with different concentration of GO doped $PCBAE_2Bz$ samples. From Fig. 17, it is very clear that the values of n_2 and β increases linearly with the corresponding increase in concentration of GO in $PCBAE_2Bz$ polymer matrix. The measured third-order NLO parameters of the prepared $PCBAE_2Bz$ and GO/$PCBAE_2Bz$ samples are presented in Table 4**.** Further, an augmentation in the optical properties for the prepared samples with higher concentration of GO was also observed, which is due the fact that the prepared composites with higher concentration GO will have more number of GO molecules that can participate in the non-linear optical process. The prepared matrix and composites in solutions are thermally agitated to excited states and consequently it is leading to improved optical properties.

Conclusion

In this study, a series of cardanol based benzoxazine monomers were synthesized by solventless method using aliphatic ether linked aromatic diamines with different chain lengths. Varying weight percentages of amine functionalized *f*-GO has been incorporated to obtain the aliphatic ether linked cardanol based polybenzoxazine composites. The Tg values and char yield of the *f*-GO/$PCBAE_nBz$ composites are significantly increased with respect to increase in the weight percentage of *f*-GO, where as Tg values decreased as the alkoxy chain length increased. The thermal stability and char yield of the composites were increased with respect to the reinforcement of *f*-GO content, while the thermal stability decreases as the aliphatic ether chain length increases. Similarly, the dielectric constant also increased in proportion to the weight percentage of *f*-GO in all the three composite systems. Antimicrobial studies proved that the neat matrix samples as well as *f*-GO reinforced composites exhibit antimicrobial activity against both gram positive and gram negative bacteria. The present study makes a conclusion that among the three *f*-GO/$PCBAE_nBz$ polybenzoxazine composites, the *f*-GO/$PCBAE_2Bz$ composite system possess better thermal, dielectric and antibacterial properties. Data resulted from different studies, it is concluded that the *f*-GO/$PCBAE_nBz$ composites developed in the present work may find wide range of applications including the field of electronics.

References

1. Mujahid M, Srivastava DS, Avasthi DK (2011) Dielectric constant and loss factor measurement of polycarbonate, Makrofol KG using swift heavy ion O^{5+}. Radiat Phys Chem 80:582–586
2. Han C, Gu A, Liang G, Yuan L (2010) Carbon nanotubes/cyanate ester composites with low percolation threshold, high dielectric constant and outstanding thermal property. Compos A: Appl Sci Manuf 41:1321–1328
3. Wang YH, Chang CM, Liu YL (2012) Benzoxazine-functionalized multi-walled carbon nanotubes for preparation of electrically-conductive polybenzoxazines. Polymer 53:106–112
4. Ishida H, Rodriguez Y (1995) Curing kinetics of a new benzoxine based phenolic resins by differential scanning calorimetr. Polymer 36:3151–3158
5. Yagci Y, Kiskan B, Ghosh NN (2009) Recent advancement on Polybenzoxazine—a newly developed high performance thermoset. J Polym Sci A Polym Chem 47:5565–5576
6. Reghunadhan Nair CP (2004) Advances in addition-cure phenolic resins. Prog Polym Sci **29**:401–498
7. Ghosh NN, Kiskan B, Yagci Y (2007) Polybenzoxazines—new high performance thermosetting resins: synthesis and properties. Prog Polym Sci 32:1344–1391
8. Xu GM, Shi T, Liu JH, Wang Q (2014) Preparation of a liquid benzoxazine based on cardanol and the thermal stability of its graphene oxide composites. J Appl Polym Sci **131**:40353–40360
9. Rao BS, Aruna P (2012) A new thermo set system based on cardanol benzoxazine and hydroxyl benzoxazoline with lower cure temperature. Prog Org Coat **74**:427–434
10. Chernykh A, Agag T, Ishida H (2009) Synthesis of linear polymers containing benzoxazine moieties in the main chain with high molecular design versatility via click reaction. Polymer 50:382–390
11. Liu Y, Zhao S, Zhang H, Wang M, Run M (2012) Synthesis, polymerization, and thermal properties of benzoxazine based on p-aminobenzonitrile. Thermochim Acta **549**:42–48
12. Andronescu C, Garea CS, Deleanu C, Iovu H (2012) Characterization and curing kinetics of new benzoxazine monomer based on aromatic diamines. Thermochim Acta 530:42–51
13. Godovsky DY (2000) Device applications of polymer-nanocomposites. Adv Polym Sci 153:163–205
14. Alexandre M, Dubois P (2000) Polymer-layered silicate nanocomposites: preparation, properties and uses of a new class of materials. Mater Sci Eng R 28:1–63
15. Ray SS, Okamoto M (2003) Polymer/layered silicate nanocomposites: a review from preparation to processing. Prog Polym Sci 28: 1539–1641
16. Kuila T, Srivastava SK, Bhowmick AK, Saxena AK (2008) Thermoplastic polyolefin based polymer-blend-layered double hydroxide nanocomposites. Compos Sci Technol 68:3234–3239
17. Zornoza B, Irusta S, Tellez C, Coronas J (2009) Mesoporous silica sphere-polysulfone mixed matrix membranes for gas separation. Langmuir 25:5903–5909
18. Uddin F (2008) Clays, Nanoclays, and montmorillonite minerals. Metall Mater Trans A 39:2804–2814

19. Renukappa NM, Siddaramaiah H, Sudhaker Samuel RD, Sundara Rajan J, Lee JH (2009) Dielectric properties of carbon black: SBR composites. J Mater Sci Mater Electron 20:648–656
20. Hong CE, Prashantha K, Advani SG, Lee JH (2007) Effects of oxidative conditions on properties of multi-wall carbon nanotubes of polymer nanocomposites. Compos Sci Technol **67**:1027–1034
21. Khanna V, Bakshi BR (2009) Carbon nanofiber polymer composites: evaluation of life cycle energy use. Environ Sci Technol 43: 2078–2084
22. Jayaraman T, Murthy A, Elakkiya V, Chandrasekaran S, Nithyadharseni P, Khan Z, Senthil R, Shanker R, Raghavender M, Kuppusami P, Jagannathan M, Ashokkumar M (2018) Recent development on carbon based heterostructures for their applications in energy and environment: a review. J Ind Eng Chem 64: 16–59
23. Liu N, Luo F, Wu H, Liu Y, Zhang C, Chen J (2008) One step ionic-liquidassisted electrochemical synthesis of ionic-liquid-functionalized graphene sheets directly from graphene. Adv Funct Mater 18:1518–1525
24. Kim H, Abdala AA, Macosko CW (2010) Graphene/polymer nanocomposites. Macromolecules **43**:6515–6530
25. Zhao X, Zhang Q, Chen D (2010) Enhanced mechanical properties of graphene-based poly(vinyl alcohol) composites. Macromolecules **43**:2357–2363
26. Yang K, Li Y, Tan X, Peng R, Liu Z (2013) Behavior and toxicity of graphene and its functionalized derivativesin biological systems. Small 9:1492–1503
27. Selvaraj V, Jayanthi KP, Alagar M (2017) Synthesis and characterization of cardanol based fluorescent composite for optoelectronic and antimicrobial applications. Polymer **108**:449–461
28. Geethakrishnan T, Palanisamy PK (2007) Z-scan determination of the third-order optical nonlinearity of a triphenylmethane dye using 633 nm He–Ne laser. Opt Commun **270**:424–428
29. Jeyaram S, Geethakrishnan T (2017) Third-order nonlinear optical properties of acid green 25 dye by Z─scan method. Opt Laser Technol **89**:179–185
30. Sahraoui B, Luc J, Meghea A, Czaplicki R, Fillaut JL, Migalska-Zalas A (2009) Nonlinear optics and surface relief gratings in alkynyl–ruthenium complexes. J Opt A Pure Appl Opt 11:024005E
31. Bredas JL, Adant C, Tackx P, Persoons A (1994) Third-order nonlinear optical response in organic materials: theoretical and experimental aspects. Chem Rev 94:243–278
32. Papagiannouli I, Iliopoulosc K, Gindre D, Sahraoui B, Krupka O, Smokal V, Kolendo A, Couris S (2012) Third-order nonlinear optical response of push–pull azobenzene polymers. Chem Phys Lett **554**:107–112
33. John Kiran A, Sathessh Raj N, Udhayakumar D, Chandrasekharan K, Kalluraya B, Philip R, Shashikala HD, Adhikari AV (2008) Nonlinear optical properties of p-(N,N-dimethylamino)dibenzylideneacetone doped polymer. Mater Res Bull **43**:707–713
34. Zongo S, Sanusi K, Britton J, Muthunzi P, Nyokong T, Maaza M, Sahraoui B (2015) Nonlinear optical properties of natural laccaic acid dye studied using Z-scan technique. Opt Mater **46**:270–275
35. Divya M, Malliga P, Sagayaraj P, Joseph Arul Pragasam A (2019) Optical based electrical properties of thiourea borate NLO crystal for electro-optic Q switches. J Electron Mater 48:5632–5639
36. Wang F, Wang G, Due HL, Li C (2008) Poly(aniline-co-o-anisidine)/sulfonated carbon nanotubes composites prepared by surface adsorption method. J Macromol Sci A **47**:743–753
37. Borole DD, Kapadi UR, Mahulikar PP, Hundiwale DG (2006) Conducting polymers: an emerging field of biosensors. Des Monomers Polym **9**:1–11
38. Allen MJ, Tung VC, Kaner RB (2010) Honeycomb carbon: A review of graphene. Chem Rev 110:132–145
39. Li L, Zhang BQ, Chen XM (2013) Dielectric characteristics of polyvinylidene fluoride-polyaniline percolative composites up to microwave frequencies. Appl Phys Lett **103**:192902
40. Olad A, Hagh HBK (2019) Graphene oxide and amin-modified graphene oxide incorporated chitosan-gelatin scaffolds as promising materials for tissue engineering. Compos Part B 162:692–702
41. García-Argumánez A, Llorente I, Caballero-Calero O, González Z, Menéndez R, Escudero ML, García-Alonso MC (2019) Electrochemical reduction of graphene oxide on biomedical grade CoCr alloy. Appl Surf Sci 465:1028–1036
42. Chen Y, Zhang X, Yu P, Ma Y (2009) Stable dispersions of graphene and highly conducting graphene films: A new approach to creating colloids of graphene monolayers. Chem Commun 45: 4527–4529
43. Chen YP, He XY, Dayo A, Wang JY, Liu WB, Wang J, Tang T (2019) Synthesis and characterization of cardanol containing tetrafunctional fluorene-based benzoxazine resin having two different oxazine ring structures. Polymer 179:121620–121626
44. Park S, Dikin D, Nguyen ST, Ruoff RS (2009) Graphene oxide sheets chemically cross-linked by polyallylamine. J Phys Chem C 113:15801–15804
45. Selvaraj V, Jayanthi KP, Lakshmikandhan T, Alagar M (2015) Development of polybenzoxazine/TSBA-15 composite from renewable resource cardanol for low k applications. RSC Adv **5**: 48898–48907
46. Zeng M, Wang J, Li R, Liu JX, Chen W, Xu Q, Gu Y (2013) The curing behavior and thermal property of graphene oxide/benzoxazine nanocomposites. Polymer 54:3107–3116
47. Suresh Kumar SM, Subramanian K (2016) Enhancement in Mechanical, Thermal, and DielectricProperties of Functionalized Graphene Oxide Reinforced Epoxy Composites. Adv Polym Technol **37**:612–621
48. Bourlinos AB, Gournis D, Petridis D, Szabo T, Szeri A, Dekany I (2003) Graphite oxide: chemical reduction to graphite and surface modification with primary aliphatic amines and amino acids. Langmuir 19:6050–6055
49. Cano-Castillo U, Rejon L (2001) AC and DC measurements of silica-carbon-reinforced polymeric current collector plate. J New Mater Electrochem Syst **4**:37–40
50. Pan S, Aksay IA (2011) Factors controlling the size of graphene oxide sheets produced *via* the graphite oxide route. ACS Nano 5: 4073–4083
51. Zheng Y, Zhang A, Chen O, Zhang J, Ning R (2006) Functionalized effect on carbon nanotube/epoxy nano-composites. Mater Sci Eng A **435–436**:145–149
52. Ramesh P, Bhagyalakshmi S, Sampath S (2004) Preparation and physicochemical and electrochemical characterization of exfoliated graphite oxide. J Colloid Interface Sci 274:95–102
53. Sheik-Bahae M, Said AA, Van Stryland EW (1989) High-sensitivity, single-beam n2 measurements. Opt Lett **14**:955–957
54. Sheik-Bahae M, Said AA, Wei T, Hagan DJ, Van Stryland EW (1990) Sensitive measurement of optical nonlinearities using a single beam. IEEE J Quantum Electron **26**:760–769
55. Christodoulides DN, Khoo IC, Salamo GJ, Stegeman GI, Van Stryland EW (2010) Nonlinear refraction and absorption: mechanisms and magnitudes. Adv Opt Photon **2**:60–200
56. Coropceanu V, Cornil J, Da DA, Filho S, Olivier Y, Silbey R, das Bre J-L (2007) Charge transport in organic semiconductors. Chem Rev **107**:926–952